Cornea

Characterization of a Novel Mouse Model for Fuchs Endothelial Corneal Dystrophy

Subashree Murugan,[1] Viviane Souza de Campos,[1] Sachin Anil Ghag,[1] Matthew Ng,[2] and Rajalekshmy Shyam[1]

[1]Vision Science Program, School of Optometry, Indiana University Bloomington, Indiana, United States
[2]Department of Biology, Indiana University Bloomington, Indiana, United States

Correspondence: Rajalekshmy Shyam, Vision Science Program, School of Optometry, Indiana University Bloomington, 800 E. Atwater Avenue, Bloomington, IN 47405, USA; rashyam@iu.edu.

Received: October 9, 2023
Accepted: March 23, 2024
Published: April 8, 2024

Citation: Murugan S, de Campos VS, Ghag SA, Ng M, Shyam R. Characterization of a novel mouse model for fuchs endothelial corneal dystrophy. *Invest Ophthalmol Vis Sci.* 2024;65(4):18. https://doi.org/10.1167/iovs.65.4.18

Purpose. Fuchs endothelial corneal dystrophy (FECD) is a progressive blinding disorder, characterized by increased corneal endothelial excrescences (guttae), corneal endothelial cell loss, and edema. These symptoms are hypothesized to be caused by changes in the extracellular matrix (ECM) and mitochondrial dysfunction in the corneal endothelium. Despite this clinical and biological relevance, a comprehensive animal model that recapitulates all the major disease characteristics is currently unavailable. In this study, we develop such a model to improve our understanding of the signaling pathways involved in the FECD progression and develop strategies for early intervention.

Method. To generate a comprehensive FECD model, we generated a double mutant mouse bearing tamoxifen-inducible knockdown of *Slc4a11* and the *Col8a2* (*Q455K*) mutation. We performed optical coherence tomography (OCT) and in vivo confocal microscopy using the Heidelberg Retinal Tomography 3 - Rostock Cornea module (HRT3-RCM) on the mice at 5 weeks of age before tamoxifen feeding to establish baseline values for corneal thickness, endothelial cell density, and test for the presence of guttae. We measured these parameters again post-tamoxifen treatment at 16 weeks of age. We collected corneas at 16 weeks to perform histopathology, immunofluorescence staining for tight junctions, adherens junctions, and oxidative stress. We evaluated endothelial pump function using a lactate assay.

Results. The double mutant tamoxifen-fed animals showed the presence of guttae, and displayed increased corneal thickness and decreased endothelial cell density. Endothelial cells showed altered morphology with disrupted adherens junctions and elevated reactive oxygen species (ROS). Finally, we found that stromal lactate concentrations were elevated in the double mutant mice, indicative of compromised endothelial pump function.

Conclusions. Overall, this mouse model recapitulates all the important phenotypic features associated with FECD.

Keywords: fuchs endothelial corneal dystrophy (FECD), corneal endothelial dystrophy, *Col8a2*, *Slc4a11*, guttae

The corneal endothelium is a non-regenerative,[1–3] metabolically active monolayer that maintains corneal transparency through stromal dehydration (deturgescence).[4–7] Endothelial degeneration and dysfunction result in bilateral noninflammatory disorders collectively classified as corneal endothelial dystrophies.[8,9] Of these disorders, Fuchs endothelial corneal dystrophy (FECD) is a progressive blinding disorder prevalent in 4% of Americans over 40 years of age.[7,9,10] Disease progression in FECD is characterized by a host of symptoms, including endothelial cell loss, increased corneal endothelial excrescences (guttae), thickening of Descemet's membrane,[11] enlarged and variable cell size of endothelial cells (polymegethism), changes in corneal endothelial morphology (pleomorphism),[12,13] and corneal edema, ultimately resulting in vision loss.[14] Corneal transplantation is the most common treatment option available.[15–17] Disadvantages of this treatment include graft rejection, a reduced survival rate of 5 years for the transplanted tissue, and secondary ocular complications like glaucoma and retinal detachment,[15] necessitating alternate treatment options.

FECD progresses longitudinally with little to no visual deficits at the initial stage. Typically, guttae are the first sign of disease,[11] followed by corneal endothelial cell loss and edema. Most studies of FECD pathogenesis are conducted on end-stage human tissues and corneal endothelial cell lines.[18–21] Although informative, they provide a limited understanding of the disease progression. Animal models can circumvent this problem; however, the prevalent mouse models for FECD represent only certain disease features. Notably, the *Col8a2 Q455K* mouse, which contains an autosomal dominant mutation implicated in early-onset FECD, shows the presence of guttae and corneal endothelial cell loss but no corneal edema.[22]

Similarly, the *Slc4a11*$^{-/-}$ is a mouse model of congenital hereditary endothelial dystrophy[23,24] and late-onset FECD[25]

Investigative Ophthalmology & Visual Science

progression. This model shows corneal edema, endothelial cell loss, and polymegethism but no guttae.[23] Whereas the *Slc4a11*$^{-/-}$ and Col8a2 *Q455K* mouse models exhibit corneal endothelial dysfunctions, these mice are otherwise healthy with no developmental abnormalities.[22,23]

The corneal endothelium is a highly metabolic cell type , and has the second highest density of mitochondria in the human body.[26,27] SLC4A11 is an inner mitochondrial membrane protein highly expressed in the corneal endothelium,[27,28] with the early-onset FECD *Col8a2 Q455K* mouse model showing reduced Slc4a11 transcript levels.[29] Previous studies have implicated mitochondrial dysfunction associated with elevated oxidative stress in FECD pathogenesis.[30–35] Thus, the *Slc4a11*$^{-/-}$ model can be used to identify the role of oxidative stress and mitochondrial dysfunctions in disease onset and progression.[27,36] However, extracellular matrix (ECM)-associated changes evidenced by guttae formation and thickening of Descemet's membrane[11,16,19] are absent in the *Slc4a11*$^{-/-}$ model.[24,27] It is worth noting here that the ECM in FECD disease pathogenesis has generally been underexplored. To address the deficiencies in the current FECD models, we sought to generate a comprehensive FECD model with a double mutant containing the loss of *Slc4a11* and the *Col8a2* knock-in mutation. We hypothesized that this double mutant would display all the phenotypes exhibited by the single mutants, thus generating a comprehensive FECD model showing guttae formation, corneal endothelial loss, and corneal edema. This comprehensive model would serve to provide a full-scale understanding on how oxidative stress and ECM-associated changes together affect FECD disease pathogenesis. Here, we characterized this comprehensive model and find that per our hypothesis, the double mutants recapitulate all the major features of FECD, including guttae formation, corneal endothelial cell loss, and corneal edema. Additionally, we describe evidence of the interplay between elevated oxidative stress and extracellular matrix changes and speculate on their contributions to FECD progression.

Materials and Methods

Generation of Transgenic Mice and Genotyping

All animal procedures were approved by the Institutional Animal Care and Use Committee (IACUC) at the Indiana University and adhered to the Association for Research in Vision and Ophthalmology (ARVO) statement for the use of animals in Ophthalmic and Vision Science research. A transgenic mouse containing two FECD mutations was generated by crossing the tamoxifen (Tm)-inducible knockdown of *Slc4a11* (*B6.Slc4a11*$^{Flox/Flox}$/*Rosa*$^{Cre\text{-}ERT2/Cre\text{-}ERT2}$) with *Col8a2* (*Q455K*) knock-in (*B6.Col8a2*$^{ki/ki}$) mice (Fig. 1A). The *Slc4a11*$^{Flox/Flox}$/*Rosa*$^{Cre\text{-}ERT2/Cre\text{-}ERT2}$ was a kind gift from the Joseph Bonanno laboratory at the Indiana University School of Optometry.[23] Heterozygous mice with *Col8a2* knock-in mutation were purchased from The Jackson Laboratory (strain #029749; Bar Harbor, ME, USA). Both mice were in C57BL/6J (B6) background.

The breeding scheme is outlined in Figure 1A. Briefly, we crossed *B6.Col8a2*$^{+/+}$ mice with *B6.Slc4a11*$^{Flox/Flox}$/*Rosa*$^{Cre\text{-}ERT2/Cre\text{-}ERT2}$ mice to obtain *B6.Slc4a11*$^{Flox/Flox}$/*Rosa*$^{Cre\text{-}ERT2/Cre\text{-}ERT2}$/*Col8a2*$^{+/+}$ at the F2 generation, hereafter referred to as single mutants (SMs). Similarly, we crossed *B6.Slc4a11*$^{Flox/Flox}$/*Rosa*$^{Cre\text{-}ERT2/Cre\text{-}ERT2}$ with *B6.Col8a2*$^{ki/ki}$ animals to obtain *B6.Slc4a11*$^{Flox/Flox}$/*Rosa*$^{Cre\text{-}ERT2/Cre\text{-}ERT2}$/*Col8a2*$^{ki/ki}$ at the F2 generation, hereafter referred to as double mutants (DMs). SMs (+Tm) and DMs (+Tm) were maintained on tamoxifen chow (#TD.130859; Envigo, West Lafayette, IN, USA) from 5 until 7 weeks of age. After this, these animals were maintained in standard chow until they were 16 weeks of age. Controls included SM (−Tm) and DM (−Tm) animals not fed tamoxifen chow and wildtype animals fed with tamoxifen chow. The mice were genotyped by sending ear punch samples for automated genotyping (Transnetyx, Cordova, TN, USA).

Total RNA Isolation, cDNA Synthesis and PCR

To test the knockdown of *Slc4a11* transcript following tamoxifen, kidneys from mice at 16 weeks of age were collected from each group to isolate total RNA using the Trizol method. The kidney samples were homogenized in 1 mL of Trizol (Ambion; catalog #15596018) using a handheld homogenizer for 10 minutes. Then, 200 µL of chloroform was added to the homogenate and mixed vigorously by hand for 15 seconds. The samples were centrifuged at 12,000 *g* for 15 minutes at 4°C, after a brief incubation of 5 minutes at room temperature. The aqueous layer was collected in a new tube and mixed with an equal volume of isopropanol by inversion. The samples were centrifuged at 12,000 *g* for 20 minutes at 4°C, after 10 minutes of incubation at room temperature. The supernatant was removed, and the pellet was washed with 1 mL 75% ethanol and vortexed for 5 seconds. The samples were centrifuged at 13,000 *g* for 10 minutes at 4°C. The pellets were air dried at room temperature and suspended in 50 µL of DNase/RNase free water. The RNA was stored at −80°C until further clean-up using RNeasy Mini kit (Qiagen; catalog #74104) per the manufacturer's protocol.

To synthesize cDNA from total RNA, a High-Capacity RNA-to-cDNA kit (Applied Biosystems; catalog #4387406) was used. Reverse transcription (RT) reaction mix was prepared by mixing 10 µL of the 2X RT buffer mix, 1 µL of RT enzyme mix, total RNA of 2 µg and nuclease-free water up to 20 µL per reaction. The RT reaction mix was aliquoted into PCR tubes and incubated at 37°C for 60 minutes. The reaction was stopped by heating to 95°C for 5 minutes and held at 4°C.

The cDNA was used to perform real-time PCR using the following primers for *Slc4a11*: Forward-TCTGGACTTCAACGCCTTCT and Reverse-GCACAAACGTGATGGAAATG and *Col8a2*: Forward-ATTCGAGGAGACCAAGGGCCTAAT and Reverse-AAGTGAGCACTGCAGTAAAGGCTG. The cDNA was amplified using Platinum Direct PCR Universal Master mix (Invitrogen; catalog #A44647100) per the manufacturer's protocol followed by gel electrophoresis.

Optical Coherence Tomography and Heidelberg Retinal Tomography 3 – Rostock Cornea Module

Anterior segment - optical coherence tomography (AS-OCT; (iVue100 Optovue, Inc., Fremont, CA, USA) was performed for pachymetry measurements and Heidelberg Retinal Tomography 3 – Rostock Cornea Module (HRT3-RCM; Heidelberg Engineering Inc., Franklin, MA, USA) for in vivo assessment of the corneal endothelium was performed. Corneal thickness measurements and endothelial assessment were done before tamoxifen treatment at 5 weeks of age (baseline) and at 16 weeks of age. The mice were

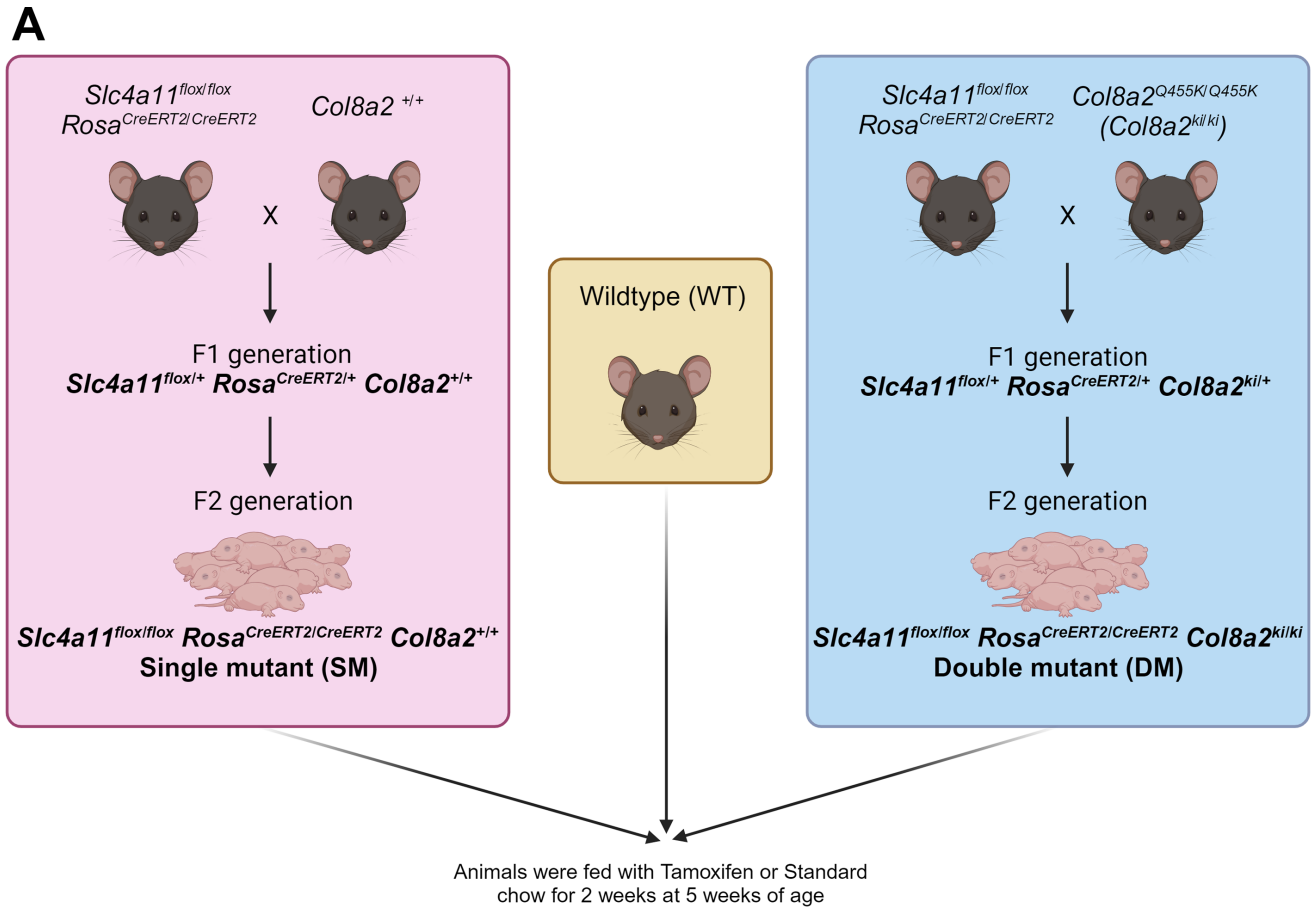

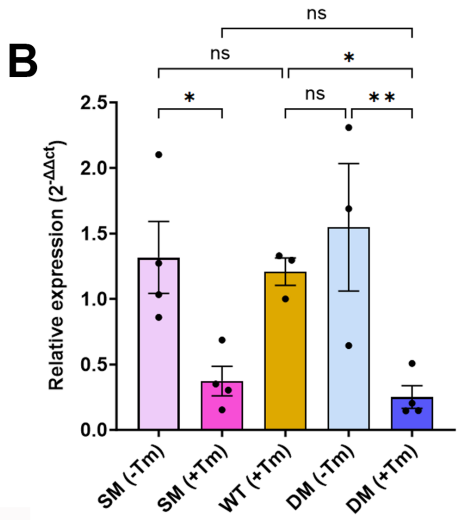

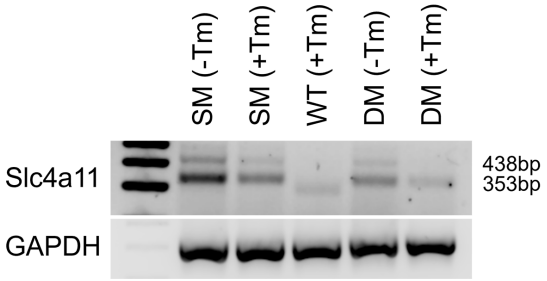

Slc4a11$^{Flox/Flox}$/Rosa$^{Cre\text{-}ERT2/Cre\text{-}ERT2}$/Col8a2$^{+/+}$ fed with Tamoxifen – SM (+Tm)
Slc4a11$^{Flox/Flox}$/Rosa$^{Cre\text{-}ERT2/Cre\text{-}ERT2}$/Col8a2$^{+/+}$ fed with normal chow – SM (-Tm)
Slc4a11$^{Flox/Flox}$/Rosa$^{Cre\text{-}ERT2/Cre\text{-}ERT2}$/Col8a2$^{ki/ki}$ fed with Tamoxifen – DM (+Tm)
Slc4a11$^{Flox/Flox}$/Rosa$^{Cre\text{-}ERT2/Cre\text{-}ERT2}$/Col8a2$^{ki/ki}$ fed with normal chow – DM (-Tm)

Figure 1. Generation of transgenic mice and verification of the *Slc4a11* knockdown. (**A**) Schematic of the gene animals. The tamoxifen-inducible knockdown of *Slc4a11* mouse (*B6.Slc4a11$^{Flox/Flox}$/Rosa$^{Cre\text{-}ERT2/Cre\text{-}ERT2}$*) was crossed either with *Col8a2* wildtype (*B6.Col8a2$^{+/+}$*) or *Col8a2 (Q455K)* knock-in (*B6.Col8a2$^{ki/ki}$*) animals to produce litters with the genotype *B6.Slc4a11$^{Flox/Flox}$/Rosa$^{Cre\text{-}ERT2/Cre\text{-}ERT2}$/Col8a2$^{+/+}$* or *B6.Slc4a11$^{Flox/Flox}$/Rosa$^{Cre\text{-}ERT2/Cre\text{-}ERT2}$/Col8a2$^{ki/ki}$* referred to as single mutants (SMs) and double mutants (DMs), respectively. The animals were either fed with tamoxifen (Tm) for 2 weeks at 5 weeks of age - SM (+Tm) or DM (+Tm), or fed with standard chow - SM (−Tm) or DM

(−Tm). Age-matched wildtype animals were also fed with Tm for 2 weeks. (**B**) Quantification of *Slc4a11* transcripts using kidney lysates from experimental SM (+Tm) or DM (+Tm), control SM (−Tm) or DM (−Tm), and wildtype (WT) animals at 16 weeks of age ($n = 3$ to 4 replicates). (**C**) The cDNA was used to perform PCR to confirm the knockdown of Slc4a11 (floxed band = 438 bp and wildtype band = 353 bp) with GAPDH as a loading control. Mean ± standard deviation (SD), ns = not significant, $^{*}P < 0.05$, $^{**}P < 0.01$, $^{****}P < 0.0001$ (1-way ANOVA with Uncorrected Fisher's LSD multiple comparisons). *B6.Slc4a11*$^{Flox/Flox}$/*Rosa*$^{Cre\text{-}ERT2/Cre\text{-}ERT2}$/*Col8a2*$^{+/+}$ fed with Tamoxifen – SM (+Tm), *B6.Slc4a11*$^{Flox/Flox}$/*Rosa*$^{Cre\text{-}ERT2/Cre\text{-}ERT2}$/*Col8a2*$^{+/+}$ fed with normal chow – SM (−Tm), *B6.Slc4a11*$^{Flox/Flox}$/*Rosa*$^{Cre\text{-}ERT2/Cre\text{-}ERT2}$/*Col8a2*$^{ki/ki}$ fed with Tamoxifen – DM (+Tm), *B6.Slc4a11*$^{Flox/Flox}$/*Rosa*$^{Cre\text{-}ERT2/Cre\text{-}ERT2}$/*Col8a2*$^{ki/ki}$ fed with normal chow – DM (−Tm).

anesthetized using a solution containing 100 mg/kg of ketamine and 10 mg/kg of xylazine, administered intraperitoneally. The ocular surface was kept moist using a saline solution during AS-OCT. Horizontal scans of the central cornea were taken using the widest pupil diameter as a reference. HRT3-RCM was done at a 400 × 400 µm field of view to obtain enface images of the corneal endothelium. Genteal eye gel (Alcon) was used to lubricate the corneal surface and as a coupling agent between the objective lens and the mouse cornea. Section scans at the corneal endothelial plane were acquired and used for assessing the number of cells and guttae.

Immunofluorescence

Corneal cups were dissected from fresh mouse eyes, washed twice with 1X phosphate buffer solution (PBS), and placed in a 96-well plate. The tissue was fixed for 10 minutes with 4% paraformaldehyde in 1X PBS at room temperature, washed with 1X PBS twice for 5 minutes, and permeabilized and blocked with 0.5% Triton X-100 (Fisher Scientific; catalog #BP151-500) and 5% normal donkey serum (Jackson Immuno Research; catalog #017-000-121) in 1X PBS for 30 minutes at room temperature. The tissues were incubated at 4°C overnight with the following primary antibodies diluted in the antibody diluent containing 0.1% Triton X-100 and 2% normal donkey serum: Mouse anti- ZO-1(Fisher Scientific; catalog #339100; 1:100), Rabbit anti-N-cadherin (Cell Signaling Technology; catalog #13116s) (1:100) and Rabbit anti-Nitrotyrosine (Life Technologies Corporation; catalog #A21285; 1:100). The tissue was washed with 1X PBS and incubated with Goat anti-Mouse IgG, Alexa Fluor 594 (Thermo Fisher; catalog #A11032) and/or Goat anti-Rabbit IgG; Alexa Fluor 488 (Thermo Fisher; catalog #A11034) secondary antibodies at 1:100 dilution for an hour at room temperature. The corneal cups were washed with 1X PBS and flat-mounted using a drop of Prolong Glass Antifade Mountant with NucBlue (Invitrogen; catalog #P36985). The tissues were imaged using a Zeiss Apotome2 microscope (Carl Zeiss, White Plains, NY, USA). One cornea from at least three animals were used for each staining condition. For nitrotyrosine stained corneas, three images of the central cornea were taken at similar laser intensity, gain, and exposure time. The images were analyzed using ImageJ to measure the mean fluorescence intensity in each image. The average staining intensity was used for statistical analysis. To study the cell shape changes, the ZO-1-stained corneal flat mount images were analyzed by manually counting and calculating the percentage of hexagonally shaped cells. Images from three different mice were used for this purpose.

Histology Staining

An affinity purified anti-peptide antibody against human SLC4A11 was designed by YenZym Antibodies (Brisbane, CA, USA) using a combination immunization strategy with 2 peptides located in the regions 614-627, and 859-875. Whole mouse eyes were enucleated, fixed in 4% PFA for 4 hours, rinsed with 1X PBS thrice, and dehydrated using graded ethanol (1 × 50%, 2 × 70%, 1 × 95%, and 2 × 100%) for 30 minutes to 1 hour each. After dehydration, the samples were transferred to citrisol for an hour, followed by wax infiltration overnight. The eyes were moved to a wax container for an hour before embedding in the cross-sectional orientation. Then, 5-micron thick sections were cut using a microtome and collected on super frost-plus slides (Fisher Scientific; catalog #22-037-246). The sections were placed at 37°C to remove the wax and then stained with Rabbit anti-Slc4a11 (YenZym Antibodies, LLC.; 1:100) after antigen retrieval using 1X citrate buffer for 30 minutes. The slides were washed with 1X PBS and incubated with Goat anti-Rabbit IgG; Alexa Fluor 488 (Thermo Fisher; catalog #A11034) secondary antibody at 1:100 dilution for an hour at room temperature. A drop of Prolong Glass Antifade Mountant with NucBlue (Invitrogen; catalog #P36985) was used to mount the sections. The sections were imaged using a Zeiss Apotome2 microscope (Carl Zeiss, White Plains, NY, USA). Images of three different sections from each group along with a no primary antibody control were obtained at similar laser intensity, gain, and exposure time. The images were analyzed using ImageJ to measure the mean fluorescence intensity at the endothelium. The average staining intensity of the no primary antibody control was subtracted from the average intensity of each group. The percent change in fluorescence intensity was plotted after normalization to the SM (−Tm) group and used for statistical analysis.

Lactate Assay

Whole corneas were isolated from mouse eyes, weighed before pulverizing using liquid nitrogen, and homogenized in 30 µL of PBS using a motor and pestle. The supernatant was separated from the pellet by centrifugation at 15,000 *g* for 15 minutes at 4°C. The supernatant was used to measure the lactate concentration using a lactate assay kit-WST (Dojindo Molecular Technologies; catalog #L256) per the manufacturer's instructions.

Capillary-Based Western Immunoassay

Post-surgical human FECD corneal endothelium (a kind gift from the Price Vision group, Indianapolis) and age-matched control (obtained from Vision First, Indianapolis) endothelial samples were pooled (at least endothelium from 2 eyes for controls and FECD samples) and lysed using 1X RIPA lysis buffer containing protease and phosphatase inhibitor with a Qsonica probe sonicator at an amplitude of 20%, 5 times for 10 seconds each, on ice. The sample was centrifuged at 13,000 *g* for 15 minutes at 4°C and the supernatant was collected. The protein concentration was measured using BCA method. A 12-230 kDa separation

module (SM-W002) of a Protein Simple Wes system was used to perform capillary-based Western immunoassay. The plate was loaded as per the manufacturer's instructions. The samples were probed with Rabbit anti-Slc4a11 (YenZym Antibodies, LLC.; 1:20) and Mouse anti-α-Tubulin (Novus Biologicals; catalog #NB100-690; 1:10) antibodies. The data obtained as electropherograms and virtual blots were normalized to the housekeeping protein.

Statistical Analysis

The quantification data was analyzed using GraphPad Prism Software (version 10.0.2; Boston, MA, USA). The bar graphs with error bars are representative of the mean and standard deviation. One-way analysis of variance (ANOVA) was performed to compare the different groups and determine statistical significance (*P* value less than or equal to of 0.05 was considered significant).

Illustrations

All illustrations were created using BioRender.com.

Results

Confirmation of *Slc4a11* Knockdown and *Col8a2* Knock-In in the Double Mutant Animals

To assess the efficacy of tamoxifen-mediated knockdown of *Slc4a11* expression, we evaluated *Slc4a11* transcript levels in SM (+Tm) and DM (+Tm) compared to SM (−Tm) and DM (−Tm). In addition to the corneal endothelium, *Slc4a11* is highly expressed in the kidneys.[28,37] Therefore, we sought to reserve the corneas for imaging analysis and examined efficiency of tamoxifen mediated knockdown of *Slc4a11* in the kidneys. The relative expression of *Slc4a11* was reduced in the SM (+Tm) and DM (+Tm) mutant animals when compared to SM (−Tm), DM (−Tm), and wildtype animals (Fig. 1B). Gel electrophoresis of PCR products showed little to no expression of the floxed allele in the SM (+Tm) and DM (+Tm) (Fig. 1C). At the same time, the animals not fed with tamoxifen, SM (−Tm) and DM (−Tm) showed the presence of the floxed and the wildtype allele. *Slc4a11* WT allele showed bands at 353 bp and floxed allele at 438 bp. The wildtype animals displayed only the wildtype band at 353 bp (see Fig. 1C). Immunofluorescence staining of histol-

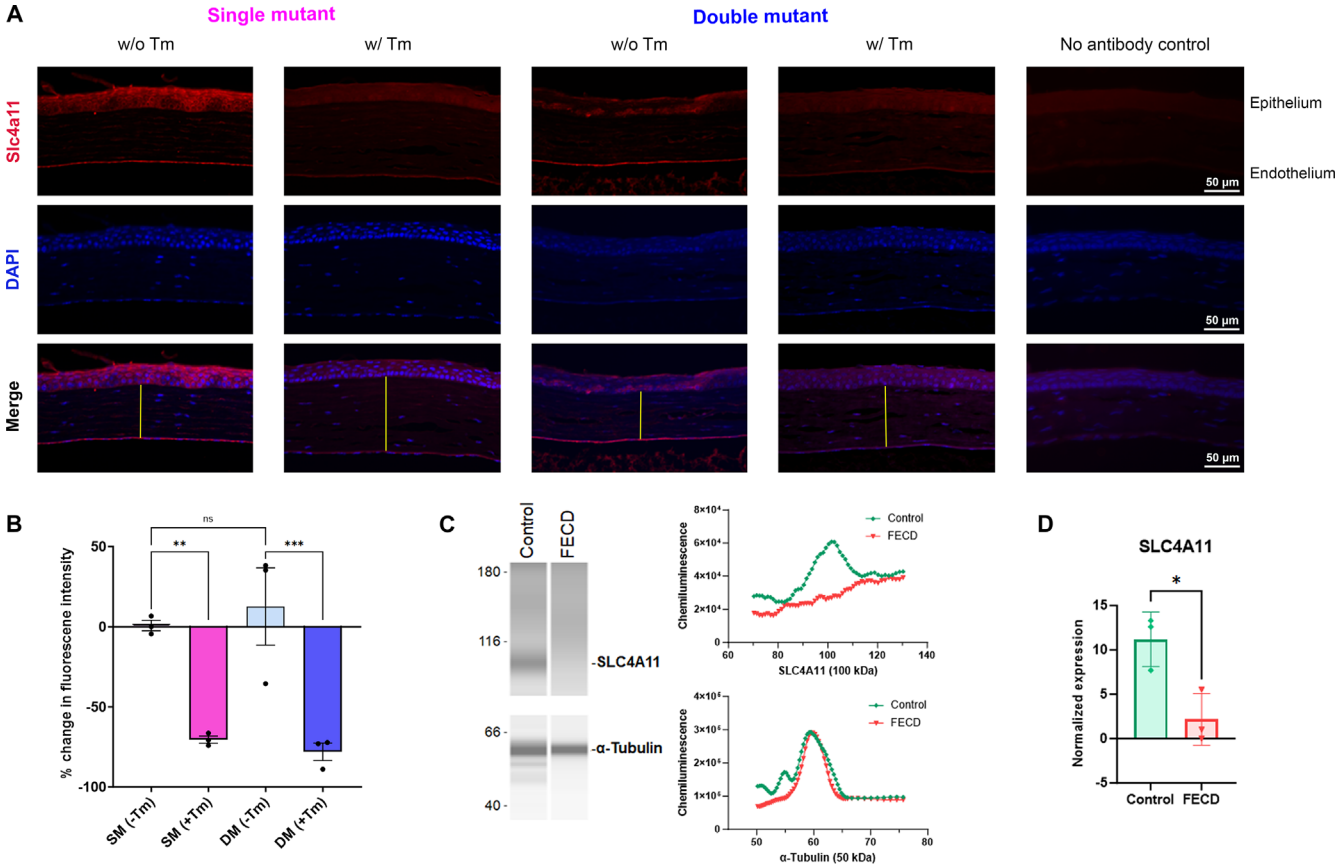

Figure 2. Immunofluorescence staining of Slc4a11 on histological sections. (**A**) Representative images of Slc4a11 expression in the corneal endothelium of SM (−Tm), SM (+Tm), WT, DM (−Tm), DM (+Tm) animals at 16 weeks of age and a no primary antibody control. *Yellow lines* represent the stromal thickness. Scale bar 50 µm. (**B**) Quantification of the percent change after subtracting the fluorescence from the no primary antibody control and normalizing to the mean fluorescence of SM (−Tm) from A ($n = 3$ eyes). Mean ± standard deviation (SD), $^{**}P < 0.01$, $^{****}P < 0.0001$ (1-way ANOVA with Uncorrected Fisher's LSD multiple comparisons). (**C**) Wes immunoassay virtual blots of SLC4A11 (100 kDa) and α-Tubulin (50 kDa) in human FECD and age-matched control samples (on the *left*) and their electropherograms (on the *right*). (**D**) Quantification of the expression of SLC4A11 normalized to α-Tubulin ($n = 3$ eyes). Mean ± standard deviation (SD), $^{*}P < 0.05$ (Unpaired t-test). *B6.Slc4a11*$^{Flox/Flox}$/*Rosa*$^{Cre\text{-}ERT2/Cre\text{-}ERT2}$/*Col8a2*$^{+/+}$ fed with Tamoxifen – SM (+Tm), *B6.Slc4a11*$^{Flox/Flox}$/*Rosa*$^{Cre\text{-}ERT2/Cre\text{-}ERT2}$/*Col8a2*$^{+/+}$ fed with normal chow – SM (−Tm), *B6.Slc4a11*$^{Flox/Flox}$/*Rosa*$^{Cre\text{-}ERT2/Cre\text{-}ERT2}$/*Col8a2*$^{ki/ki}$ fed with Tamoxifen – DM (+Tm), *B6.Slc4a11*$^{Flox/Flox}$/*Rosa*$^{Cre\text{-}ERT2/Cre\text{-}ERT2}$/*Col8a2*$^{ki/ki}$ fed with normal chow – DM (−Tm).

ogy sections showed approximately 70% reduction in the expression of Slc4a11 in the SM (+Tm) and DM (+Tm) (Figs. 2A, 2B). Capillary-based Jess immunoassay showed a significant reduction in SLC4A11 protein expression in human FECD samples when compared to age-matched controls (Figs. 2C, 2D).

Elevated Corneal Edema and Lactate Content in the Double Mutant Animals

One of the characteristic features of FECD is the increase in corneal thickness due to stromal edema. Histological staining of the corneal sections confirmed stromal edema in SM (+Tm) and DM (+Tm) animals (see Fig. 2A). In addition, we conducted pachymetry measurements using OCT on the animals at 5 weeks (baseline) and 16 weeks to determine any changes in corneal thickness. We observed a significant difference in corneal thickness in the SM (+Tm) and DM (+Tm) animals at 16 weeks of age when compared to their baseline measurements (Figs. 3A, 3B). On average, the SM (+Tm) and the DM (+Tm) showed approximately 50 µm increase in corneal thickness. No significant elevation in corneal thickness was observed in the wildtype animals, SM (−Tm), and DM (−Tm) (see Figs. 3A, 3B).

Corneal edema is directly proportional to the lactate accumulation resulting from the decrease in the efflux of lactate from the stroma.[38–40] Consistent with the pachymetry results, we observed an elevation in the lactate concentration in the SM (+Tm) and double DM (+Tm) when compared to the controls. In both SM (+Tm) and DM (+Tm) animals, we observed nearly 50% elevation of the lactate concentration when compared to the controls (Fig. 3C).

Decreased Corneal Endothelial Cell Count and Increased Guttae Formation in the Double Mutant Animals

FECD is characterized by the loss of corneal endothelial cells and an elevation in guttae formation.[5,7,13,41] We assessed the corneal endothelium using HRT3-RCM (Figs. 3D–F) to determine changes in corneal endothelial density and guttae. Compared to the baseline measurements at 5 weeks of age, we saw a significant decrease in cell density with a loss less than 1000 cells/mm^2 in the DM (+Tm) animals (see Figs . 3D, 3E). On the other hand, control animals lost approximately 500 cells/mm^2 (see Figs. 3D, 3E), consistent with the age-related loss of corneal endothelial density seen in humans.[3,42–44] Thus, we were able to exclude the effect of Tm on endothelial cell loss. Interestingly, the guttae numbers were comparable between DM (+Tm) and DM (−Tm), with both groups showing approximately seven guttae per captured image area on average (see Figs. 3D, 3F). As expected, SM (+Tm) and wildtype animals showed very few guttae in our analysis (see Figs. 3D, 3F).

Changes in the Adherens Junction and Hexagonality of the Endothelial Cells in the Double Mutants

N-cadherin is a major component of the adherens junctions in the corneal endothelial cells.[45,46] Cell adhesion is essen-

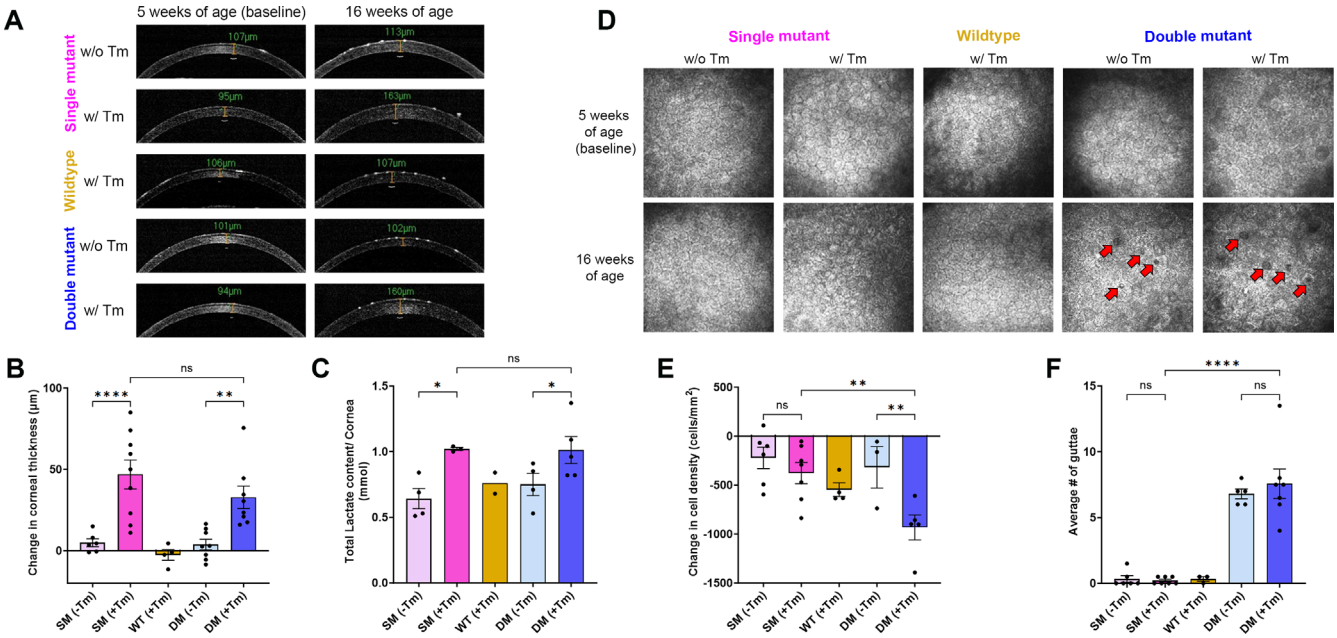

Figure 3. Phenotypic assessment. (**A**) Representative OCT images of SM (−Tm), SM (+Tm), WT, DM (−Tm), and DM (+Tm) animals at 5 weeks of age (baseline) and at 16 weeks of age. (**B**) Quantification of the change in corneal thickness at 16 weeks of age from baseline (n = 4 to 9 eyes). (**C**) Quantification of lactate content (n = 2 to 5 eyes). (**D**) Representative HRT3-RCM images of SM (−Tm), SM (+Tm), WT, DM (−Tm), and DM (+Tm) corneal endothelium (FOV 400 um) at 5 weeks of age (baseline) and 16 weeks of age; *red arrows* point to guttae. (**E**) Quantification of the change in the endothelial cell density at 16 weeks of age from baseline (n = 3 to 7 eyes). (**F**) Quantification of the average number of guttae in the right and left eyes (n = 3 to 7 eyes); Mean ± standard deviation (SD), ns = not significant, *P < 0.05, **P < 0.01, ****P < 0.0001 (1-way ANOVA with Uncorrected Fisher's LSD multiple comparisons). *B6.Slc4a11*$^{Flox/Flox}$/*Rosa*$^{Cre\text{-}ERT2/Cre\text{-}ERT2}$/*Col8a2*$^{+/+}$ fed with Tamoxifen – SM (+Tm), *B6.Slc4a11*$^{Flox/Flox}$/*Rosa*$^{Cre\text{-}ERT2/Cre\text{-}ERT2}$/*Col8a2*$^{+/+}$ fed with normal chow – SM (−Tm), *B6.Slc4a11*$^{Flox/Flox}$/*Rosa*$^{Cre\text{-}ERT2/Cre\text{-}ERT2}$/*Col8a2*$^{ki/ki}$ fed with Tamoxifen – DM (+Tm), *B6.Slc4a11*$^{Flox/Flox}$/*Rosa*$^{Cre\text{-}ERT2/Cre\text{-}ERT2}$/*Col8a2*$^{ki/ki}$ fed with normal chow – DM (−Tm).

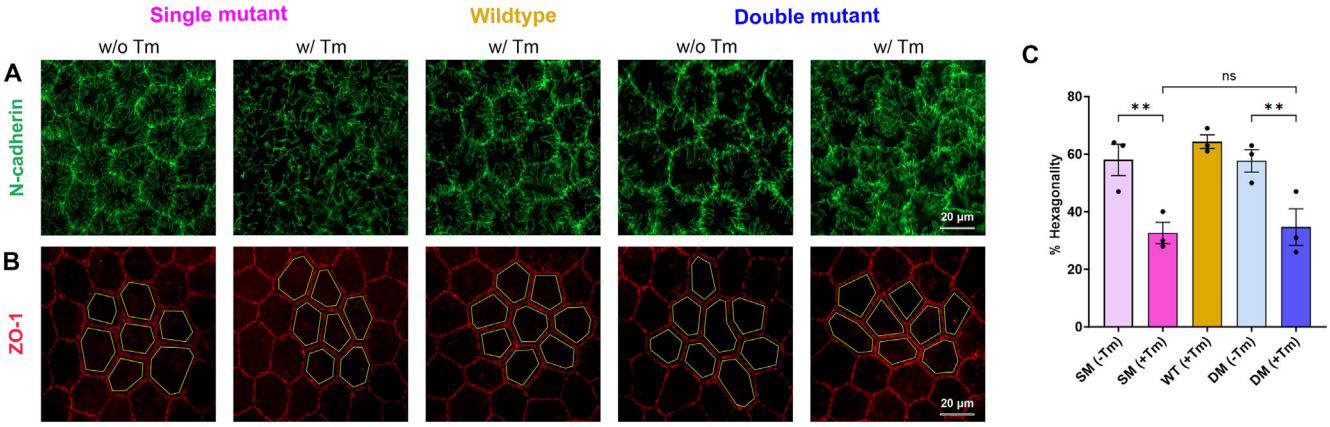

Figure 4. Evaluation of adherens junctions and cell morphology in corneal endothelial flatmounts. (**A**) Representative images of N-cadherin staining to visualize adherens junction in the corneal endothelium of SM (−Tm), SM (+Tm), WT, DM (−Tm), and DM (+Tm) animals at 16 weeks of age (n = 3 eyes). (**B**) Representative images of ZO-1 staining to visualize the endothelial cell morphology and hexagonality in SM (−Tm), SM (+Tm), WT, DM (−Tm), and DM (+Tm) animals at 16 weeks of age (n = 3 eyes). *Yellow lines* are presented to visualize the hexagonality of the endothelial cells. Scale bar 20 µm. (**C**) Quantification of the percent of hexagonal cells at 16 weeks of age. Mean ± standard deviation (SD), ns = not significant, $^{**}P < 0.01$ (1-way ANOVA with Uncorrected Fisher's LSD multiple comparisons). *B6.Slc4a11*$^{Flox/Flox}$/*Rosa*$^{Cre\text{-}ERT2/Cre\text{-}ERT2}$/*Col8a2*$^{+/+}$ fed with Tamoxifen – SM (+Tm), *B6.Slc4a11*$^{Flox/Flox}$/*Rosa*$^{Cre\text{-}ERT2/Cre\text{-}ERT2}$/*Col8a2*$^{+/+}$ fed with normal chow – SM (−Tm), *B6.Slc4a11*$^{Flox/Flox}$/*Rosa*$^{Cre\text{-}ERT2/Cre\text{-}ERT2}$/*Col8a2*$^{ki/ki}$ fed with Tamoxifen – DM (+Tm), *B6.Slc4a11*$^{Flox/Flox}$/*Rosa*$^{Cre\text{-}ERT2/Cre\text{-}ERT2}$/*Col8a2*$^{ki/ki}$ fed with normal chow – DM (−Tm).

tial in the maintenance of corneal endothelial cell integrity and function.[47] We, therefore, checked if there were disruptions in the N-cadherin expression patterns in the animals. Immunofluorescence of the corneal cups revealed highly disrupted adherens junction (Fig. 4A) in the SM (+Tm) and DM (+Tm). In contrast, we observed well-organized staining patterns in the SM (−Tm), DM (−Tm), and WT animals.

Loss of hexagonality and cell size changes are associated with FECD.[35] We carried out ZO-1 staining to assess changes to cell morphology. A regular pattern of cellular arrangements and cell size was evident in the corneal endothelium of wildtype and SM (−Tm) animals based on ZO-1 staining (Fig. 4B). However, in both DM (+Tm) and DM (−Tm) animals, we observed comparable changes in cell morphology, including the loss of hexagonal shape and cell size changes (see Fig. 4B). There was approximately a 30% decrease in the hexagonal cells in the SM (+Tm) and DM (+Tm) when compared to the SM (−Tm), DM (−Tm), and WT animals (Fig. 4C).

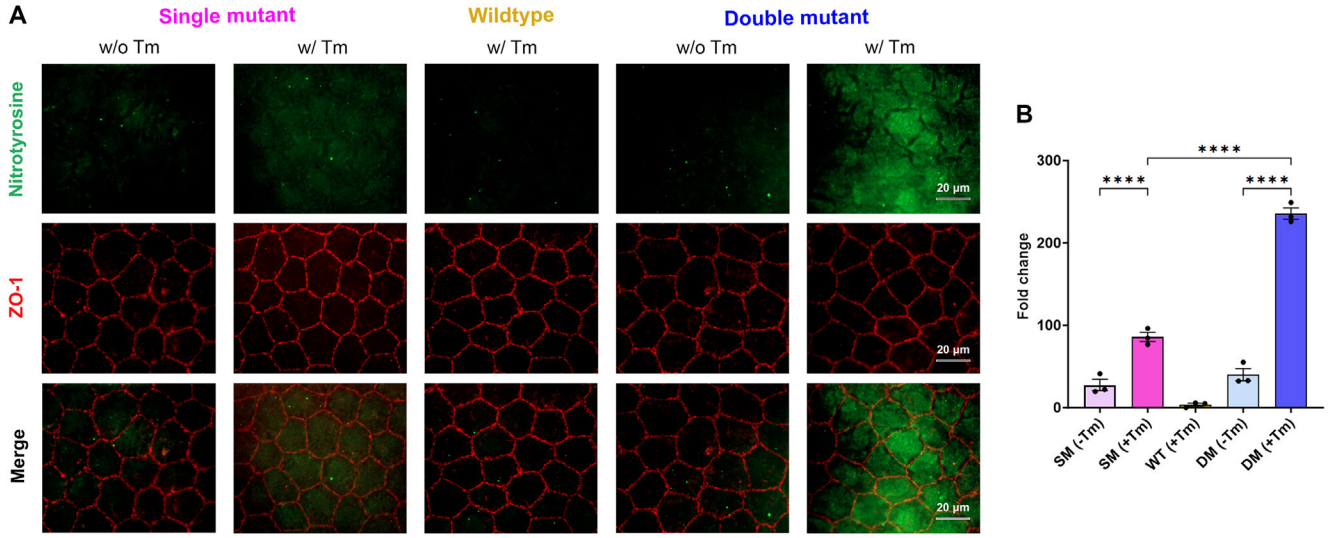

Figure 5. Evaluation of oxidative stress in corneal endothelium flat mounts. (**A**) Representative nitrotyrosine, ZO-1, and merge images to visualize the reactive oxygen species in the corneal endothelium SM (−Tm), SM (+Tm), WT, DM (−Tm), and DM (+Tm) animals at 16 weeks of age. Scale bar 20 µm. (**B**) Quantification of the fold change in mean fluorescence from **A** (n = 3 eyes). Mean ± standard deviation (SD), $^{****}P < 0.0001$ (1-way ANOVA with Uncorrected Fisher's LSD multiple comparisons). *B6.Slc4a11*$^{Flox/Flox}$/*Rosa*$^{Cre\text{-}ERT2/Cre\text{-}ERT2}$/*Col8a2*$^{+/+}$ fed with Tamoxifen – SM (+Tm), *B6.Slc4a11*$^{Flox/Flox}$/*Rosa*$^{Cre\text{-}ERT2/Cre\text{-}ERT2}$/*Col8a2*$^{+/+}$ fed with normal chow – SM (−Tm), *B6.Slc4a11*$^{Flox/Flox}$/*Rosa*$^{Cre\text{-}ERT2/Cre\text{-}ERT2}$/*Col8a2*$^{ki/ki}$ fed with Tamoxifen – DM (+Tm), *B6.Slc4a11*$^{Flox/Flox}$/*Rosa*$^{Cre\text{-}ERT2/Cre\text{-}ERT2}$/*Col8a2*$^{ki/ki}$ fed with normal chow – DM (−Tm).

Elevated Oxidative Stress in the Double Mutant Corneal Endothelium

Nitrotyrosine is a marker for elevated oxidative stress. Because FECD pathogenesis is associated with increased oxidative stress, we evaluated if there were changes in nitrotyrosine expression in the corneal endothelium of the double mutants. As expected, the SM (−Tm) and the WT animals showed minimal nitrotyrosine staining. Increased staining was evident in SM (+Tm), confirming previous findings.[23] Interestingly, we observed a nearly four-fold increase in nitrotyrosine staining in the DM (+Tm) compared to the SM (+Tm) (Figs. 5A, 5B).

Discussion

In this study, we characterized the double mutant mouse model encompassing all the disease phenotypes associated with FECD. One of the first signs of FECD is the presence of guttae, followed by corneal endothelial cell loss and corneal edema.[11,16,19] In the double mutant mouse, we observed guttae formation, corneal endothelial cell loss, and edema, which recapitulates FECD in human patients (Figs. 6A, 6B). Decrease in *Slc4a11* expression is described in the early onset FECD mouse model, *Col8a2 Q455K*[29] and in samples from patients with late onset FECD[38] highlighting the importance of this protein in disease pathogenesis. Pioneering

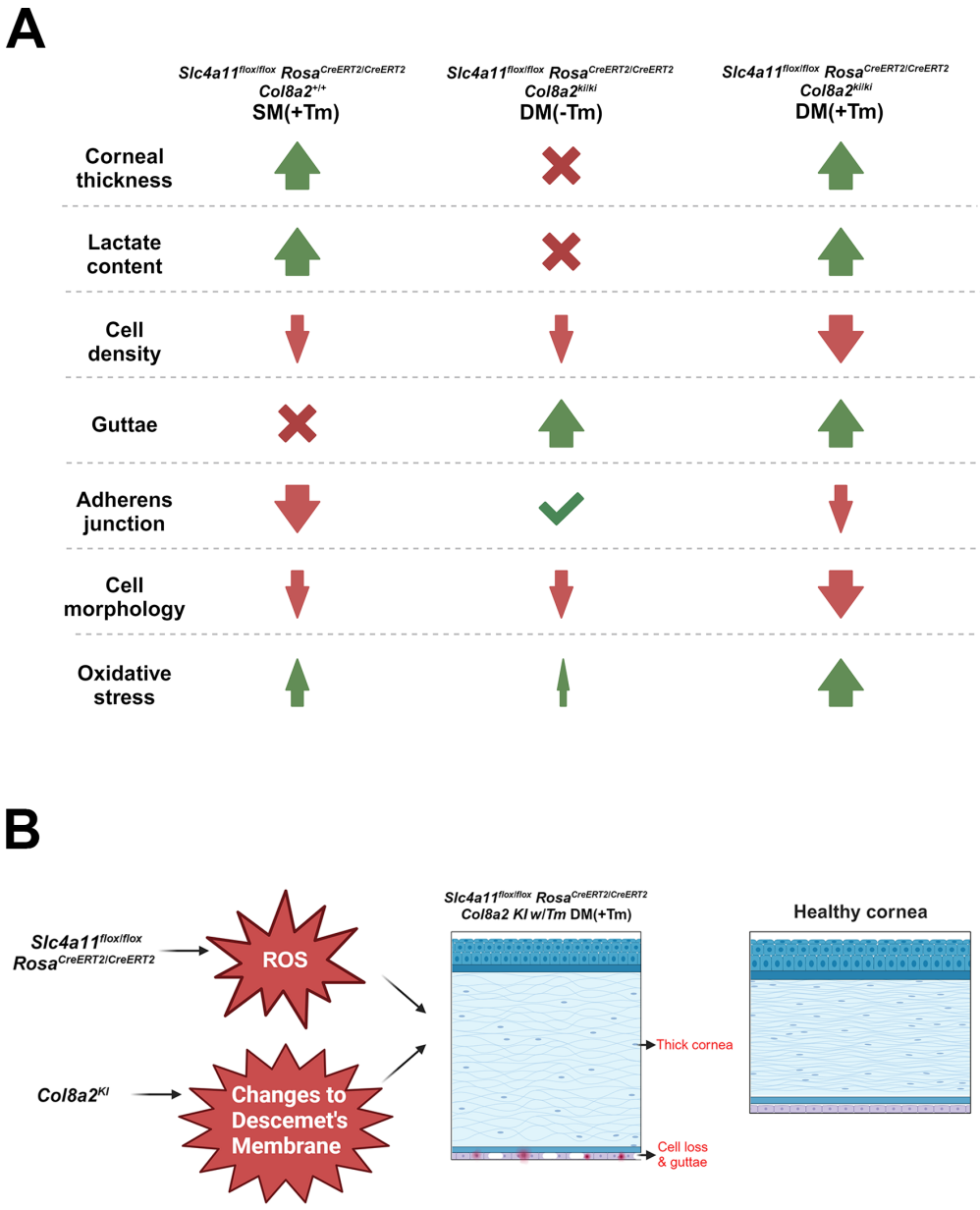

Figure 6. (**A**) Summary of the characteristic features noted in the experimental and control animals in Fuchs endothelial corneal dystrophy. The double mutant showed a significant reduction in cell density, N-cadherin expression, and cell morphology when compared to *Slc4a11* knockdown and *Col8a2* knock-in mutation. Guttae formation was comparable between *Col8a2 Q455K* knock-in mutants and the double mutant. Significant elevation in oxidative stress was evident in the double mutant when compared to *Slc4a11* knockdown. (**B**) Schematic showing the effect of the *Slc4a11* knock down and *Col8a2* knock in mutations in the *B6.Slc4a11*$^{Flox/Flox}$/*Rosa*$^{Cre\text{-}ERT2/Cre\text{-}ERT2}$/*Col8a2*$^{ki/ki}$ DM (+Tm) mouse model.

studies using immortalized corneal endothelial cells and end-stage disease tissues showed that elevated oxidative stress is a cause of FECD progression.[18–20,39] However, the lack of in vivo evidence limited the understanding of how oxidative stress can lead to the disease. The loss of *SLC4A11* elevates oxidative stress in the corneal endothelium,[31,33,36] and in mice, the loss of this gene results in corneal edema.[23] Therefore, we sought to create the double mutant to evaluate the role of elevated oxidative stress in FECD disease pathogenesis.

To study this, we considered if a temporal increase in oxidative stress with the tamoxifen-induced loss of *Slc4a11* would exacerbate the FECD phenotypes in the *Col8a2 Q455K* mouse model. We saw earlier occurrence of phenotypes and all the FECD-associated phenotypes in the DM (+Tm), which indicate the importance of oxidative stress in disease occurrence. Interestingly, while in the DM (+Tm), we observed a nearly four-fold increase in nitrotyrosine staining compared to SM (+Tm), corneal edema remained comparable between these groups of animals. This finding suggests that the upregulation of oxidative stress alone may not be causal to corneal edema.

Central corneal guttae are one of the first features associated with FECD in humans. Progressive guttae are present in the *Col8a2 Q455K* mice[22] but not in the *Slc4a11*$^{-/-}$ animals. Although the DM (+Tm) showed guttae before corneal edema or corneal endothelial cell loss (data not shown), we did not observe a significant increase in the guttae numbers between the double mutant animals (DM [+Tm]) and the *Col8a2 Q455K* littermate (DM [-Tm]) controls. This finding suggests that elevated oxidative stress might not be causal in guttae formation. Future analysis of this mouse model will help identify the signaling pathways associated with guttae formation.

YAP/TAZ signaling pathways regulate cell shape changes.[48] Polymegethism is a characteristic feature of FECD.[12,13] To identify whether the loss of TAZ, a key mechanotransducer, would result in corneal endothelial dysfunctions, Thomasy and colleagues used a knockout mouse model of *Wwrt1*.[49] This mouse model presented decreased corneal endothelial cell numbers, shape changes, and a softer Descemet's membrane, among the characteristic features of FECD. This study reveals the role of *Wwtr1* in corneal endothelial homeostasis.[49] However, corneal thinning and the absence of guttae in the *Wwrt1*$^{-/-}$ animal model indicate that it may not alone be responsible for the FECD disease phenotypes. Whether the cell shape changes observed in the double mutant animals arise due to aberrant mechanotransduction can be evaluated in future studies.

Whereas the double mutant provides all of the FECD signs, it is not a genotype specific to FECD in humans. Mutations in *Slc4a11* are implicated in late-onset FECD,[25,39] whereas *Col8a2 Q455K* mutation is associated with early-onset FECD.[22] Although the age of onset is different between these two types of FECD, the presentation and the disease progression remain remarkably similar. In this study, our goal was to challenge the early onset FECD mouse model (*Col8a2 Q455K*) with elevated oxidative stress (with *Slc4a11* knock-down) to see if it would increase the severity or hasten the occurrence of the phenotypes. We show that when challenged with oxidative stress, the *Col8a2 Q455K* mouse presents all the FECD phenotypes. Moreover, we find that the phenotypes are evident sooner in the double mutant than in the *Col8a2 Q455K* mouse. FECD is a multifactorial disease, and animal models can seldom capture all the intricacies associated with the disease process. To date, the double mutant is the only comprehensive mouse model encompassing all the phenotypes and the disease progression. It, therefore, presents an opportunity for future studies to understand the cellular mechanisms that lead to guttae formation and corneal edema.

Corneal transplantation is the treatment option available for patients with FECD in the United States. Descemet stripping automated endothelial keratoplasty (DSAEK) is a prevalent form of posterior lamellar corneal transplantation.[50] However, this is an expensive procedure, costing over $12,000 per transplant. Graft-related complications arise approximately 5% of the time, and graft rejection is expected in around 4% of the cases.[51] Cell injection therapy is gaining traction as a corneal endothelial dystrophy treatment in Japan, with improved visual acuity 5 years after the procedure.[52] However, in their 5-year follow-up study, the authors indicate that guttae persist in the corneal endothelial junctions.[53] Because the effects of guttae on cell functions are yet to be understood, the long-term efficacy of this approach will require further evaluation. In this regard, the double mutant animal model can provide insights into understanding the changes to cellular dynamics associated with guttae formation.

Conclusions

The double *Slc4a11* knock-out and *Col8a2* knock-in mutant mouse model described here encompasses the two gene mutations reported in human patients. Characterization of the double mutant mouse model showed all the main features of FECD. FECD is a multifactorial disease with genetic and environmental causes. A limitation of the double mutant mouse model is that it does not represent a specific genotype associated with FECD. However, our analysis highlights that the double mutant is a significant advancement over the prevalent animal models. Future studies will evaluate this animal model to study the pathways involved in FECD disease onset and progression.

Acknowledgments

The authors thank Joseph Bonanno, Mallika Valapala, and S.P. Srinivas (Indiana University Bloomington) for their valuable input throughout this project, and Marianne Price (Price Vision group, Indianapolis) for the FECD samples. We are grateful for the critical feedback on this manuscript from Krishnakumar Kizhatil (Ohio State University), Deepika Vasudevan (University of Pittsburgh), and Elizabeth Zuniga-Sanchez (Baylor College of Medicine). We completed this project with funding support from NIH R00 EY032974.

Supported by National Institutes of Health (R00 EY032974 to R.S.).

Disclosure: **S. Murugan**, None; **V.S. de Campos**, None; **S.A. Ghag**, None; **M. Ng**, None; **R. Shyam**, None

References

1. Feizi S. Corneal endothelial cell dysfunction: etiologies and management. *Ophthalmol Eye Dis*. 2018;10:2515841418815802.
2. Engelmann K, Böhnke M, Friedl P. Isolation and long-term cultivation of human corneal endothelial cells. *Invest Ophthalmol Vis Sci*. 1988;29(11):1656–1662.

3. Joyce NC, Meklir B, Joyce SJ, Zieske JD. Cell cycle protein expression and proliferative status in human corneal cells. *Invest Ophthalmol Vis Sci*. 1996;37(4):645–655.
4. Riley MV, Winkler BS, Starnes CA, Peters MI, Dang L. Regulation of corneal endothelial barrier function by adenosine, cyclic AMP, and protein kinases. *Invest Ophthalmol Vis Sci*. 1998;39(11):2076–2084.
5. Bourne WM. Biology of the corneal endothelium in health and disease. *Eye (Lond)*. 2003;17(8):912–918.
6. Fischbarg J, Maurice DM. An update on corneal hydration control. *Exp Eye Res*. 2004;78(3):537–541.
7. Wilson SE, Bourne WM. Fuchs' dystrophy. *Cornea*. 1988;7(1):2–18.
8. Fuchs E. Dystrophia epithelialis corneae. *Graefes Arhiv für Ophthalmologie*. 1910;76(3):478–508.
9. Schmedt T, Silva MM, Ziaei A, Jurkunas U. Molecular bases of corneal endothelial dystrophies. *Exp Eye Res*. 2012;95(1):24–34.
10. Krachmer JH, Purcell JJ, Young CW, Bucher KD. Corneal endothelial dystrophy. A study of 64 families. *Arch Ophthalmol*. 1978;96(11):2036–2039.
11. Hogan MJ, Wood I, Fine M. Fuchs' endothelial dystrophy of the cornea. 29th Sanford Gifford Memorial lecture. *Am J Ophthalmol*. 1974;78(3):363–383.
12. Polack FM. The posterior corneal surface in Fuchs' dystrophy. Scanning electron microscope study. *Invest Ophthalmol*. 1974;13(12):913–922.
13. Waring GO, Rodrigues MM, Laibson PR. Corneal dystrophies. II. Endothelial dystrophies. *Surv Ophthalmol*. 1978;23(3):147–168.
14. Kannabiran C, Chaurasia S, Ramappa M, Mootha VV. Update on the genetics of corneal endothelial dystrophies. *Indian J Ophthalmol*. 2022;70(7):2239–2248.
15. Matthaei M, Hribek A, Clahsen T, Bachmann B, Cursiefen C, Jun AS. Fuchs endothelial corneal dystrophy: clinical, genetic, pathophysiologic, and therapeutic aspects. *Annu Rev Vis Sci*. 2019;5:151–175.
16. Nanda GG, Alone DP. REVIEW: current understanding of the pathogenesis of Fuchs' endothelial corneal dystrophy. *Mol Vis*. 2019;25:295–310.
17. Zhang J, McGhee CNJ, Patel DV. The molecular basis of Fuchs' endothelial corneal dystrophy. *Mol Diagn Ther*. 2019;23(1):97–112.
18. Miyai T, Vasanth S, Melangath G, et al. Activation of PINK1-parkin-mediated mitophagy degrades mitochondrial quality control proteins in Fuchs endothelial corneal dystrophy. *Am J Pathol*. 2019;189(10):2061–2076.
19. Okumura N, Hashimoto K, Kitahara M, et al. Activation of TGF-beta signaling induces cell death via the unfolded protein response in Fuchs endothelial corneal dystrophy. *Sci Rep*. 2017;7(1):6801.
20. Yagi-Yaguchi Y, Yamaguchi T, Higa K, et al. Association between corneal endothelial cell densities and elevated cytokine levels in the aqueous humor. *Sci Rep*. 2017;7(1):13603.
21. Pan P, Weisenberger DJ, Zheng S, et al. Aberrant DNA methylation of miRNAs in Fuchs endothelial corneal dystrophy. *Sci Rep*. 2019;9:16385.
22. Jun AS, Meng H, Ramanan N, et al. An alpha 2 collagen VIII transgenic knock-in mouse model of Fuchs endothelial corneal dystrophy shows early endothelial cell unfolded protein response and apoptosis. *Hum Mol Genet*. 2012;21(2):384–393.
23. Ogando DG, Shyam R, Kim ET, Wang YC, Liu CY, Bonanno JA. Inducible Slc4a11 knockout triggers corneal edema through perturbation of corneal endothelial pump. *Invest Ophthalmol Vis Sci*. 2021;62(7):28.
24. Han SB, Ang HP, Poh R, et al. Mice with a targeted disruption of Slc4a11 model the progressive corneal changes of congenital hereditary endothelial dystrophy. *Invest Ophthalmol Vis Sci*. 2013;54(9):6179–6189.
25. Riazuddin SA, Vithana EN, Seet LF, et al. Missense mutations in the sodium borate cotransporter SLC4A11 cause late-onset Fuchs corneal dystrophy. *Hum Mutat*. 2010;31(11):1261–1268.
26. Bonanno JA, Shyam R, Choi M, Ogando DG. The H+ transporter SLC4A11: roles in metabolism, oxidative stress and mitochondrial uncoupling. *Cells*. 2022;11(2):197.
27. Ogando DG, Choi M, Shyam R, Li S, Bonanno JA. Ammonia sensitive SLC4A11 mitochondrial uncoupling reduces glutamine induced oxidative stress. *Redox Biol*. 2019;26:101260.
28. Choi M, Bonanno JA. Mitochondrial targeting of the ammonia-sensitive uncoupler SLC4A11 by the chaperone-mediated carrier pathway in corneal endothelium. *Invest Ophthalmol Vis Sci*. 2021;62(12):4.
29. Matthaei M, Hu J, Meng H, et al. Endothelial cell whole genome expression analysis in a mouse model of early-onset Fuchs' endothelial corneal dystrophy. *Invest Ophthalmol Vis Sci*. 2013;54(3):1931–1940.
30. Gendron SP, Thériault M, Proulx S, Brunette I, Rochette PJ. Restoration of mitochondrial integrity, telomere length, and sensitivity to oxidation by in vitro culture of Fuchs' endothelial corneal dystrophy cells. *Invest Ophthalmol Vis Sci*. 2016;57(14):5926–5934.
31. Czarny P, Seda A, Wielgorski M, et al. Mutagenesis of mitochondrial DNA in Fuchs endothelial corneal dystrophy. *Mutat Res*. 2014;760:42–47.
32. Halilovic A, Schmedt T, Benischke AS, et al. Menadione-induced DNA damage leads to mitochondrial dysfunction and fragmentation during rosette formation in Fuchs endothelial corneal dystrophy. *Antioxid Redox Signal*. 2016;24(18):1072–1083.
33. Jurkunas UV, Bitar MS, Funaki T, Azizi B. Evidence of oxidative stress in the pathogenesis of Fuchs endothelial corneal dystrophy. *Am J Pathol*. 2010;177(5):2278–2289.
34. Katikireddy KR, White TL, Miyajima T, et al. NQO1 downregulation potentiates menadione-induced endothelial-mesenchymal transition during rosette formation in Fuchs endothelial corneal dystrophy. *Free Radic Biol Med*. 2018;116:19–30.
35. Ong Tone S, Kocaba V, Bohm M, Wylegala A, White TL, Jurkunas UV. Fuchs endothelial corneal dystrophy: the vicious cycle of Fuchs pathogenesis. *Prog Retin Eye Res*. 2021;80:100863.
36. Guha S, Chaurasia S, Ramachandran C, Roy S. SLC4A11 depletion impairs NRF2 mediated antioxidant signaling and increases reactive oxygen species in human corneal endothelial cells during oxidative stress. *Sci Rep*. 2017;7(1):4074.
37. Kao L, Azimov R, Shao XM, et al. Multifunctional ion transport properties of human SLC4A11: comparison of the SLC4A11-B and SLC4A11-C variants. *Am J Physiol Cell Physiol*. 2016;311(5):C820–C830.
38. Gottsch JD, Bowers AL, Margulies EH, et al. Serial analysis of gene expression in the corneal endothelium of Fuchs' dystrophy. *Invest Ophthalmol Vis Sci*. 2003;44(2):594–599.
39. Vithana EN, Morgan PE, Ramprasad V, et al. SLC4A11 mutations in Fuchs endothelial corneal dystrophy. *Human Molecular Genetics*. 2008;17(5):656–666.
40. Li S, Kim E, Ogando DG, Bonanno JA. Corneal endothelial pump coupling to lactic acid efflux in the rabbit and mouse. *Invest Ophthalmol Vis Sci*. 2020;61(2):7.
41. Elhalis H, Azizi B, Jurkunas UV. Fuchs endothelial corneal dystrophy. *Ocul Surf*. 2010;8(4):173–184.

42. McCarey BE, Edelhauser HF, Lynn MJ. Review of corneal endothelial specular microscopy for FDA clinical trials of refractive procedures, surgical devices, and new intraocular drugs and solutions. *Cornea*. 2008;27(1):1–16.
43. Joyce NC. Proliferative capacity of corneal endothelial cells. *Exp Eye Res*. 2012;95(1):16–23.
44. Mohammad-Salih PAK. Corneal endothelial cell density and morphology in normal Malay eyes. *Med J Malaysia*. 2011;66(4):300–303.
45. Vassilev VS, Mandai M, Yonemura S, Takeichi M. Loss of N-cadherin from the endothelium causes stromal edema and epithelial dysgenesis in the mouse cornea. *Invest Ophthalmol Vis Sci*. 2012;53(11):7183–7193.
46. Thériault M, Gendron SP, Brunette I, Rochette PJ, Proulx S. Function-related protein expression in Fuchs endothelial corneal dystrophy cells and tissue models. *Am J Pathol*. 2018;188(7):1703–1712.
47. Srinivas SP. Cell signaling in regulation of the barrier integrity of the corneal endothelium. *Exp Eye Res*. 2012;95(1):8–15.
48. Piccolo S, Dupont S, Cordenonsi M. The biology of YAP/TAZ: hippo signaling and beyond. *Physiol Rev*. 2014;94(4):1287–1312.
49. Leonard BC, Park S, Kim S, et al. Mice deficient in TAZ (Wwtr1) demonstrate clinical features of late-onset Fuchs' endothelial corneal dystrophy. *Invest Ophthalmol Vis Sci*. 2023;64(4):22.
50. Price MO, Mehta JS, Jurkunas UV, Price FW. Corneal endothelial dysfunction: evolving understanding and treatment options. *Prog Retin Eye Res*. 2021;82:100904.
51. Yong KL, Nguyen HV, Cajucom-Uy HY, et al. Cost minimization analysis of precut cornea grafts in descemet stripping automated endothelial keratoplasty. *Medicine (Baltimore)*. 2016;95(8):e2887.
52. Kinoshita S, Koizumi N, Ueno M, et al. Injection of cultured cells with a ROCK inhibitor for bullous keratopathy. *N Engl J Med*. 2018;378(11):995–1003.
53. Numa K, Imai K, Ueno M, et al. Five-year follow-up of first 11 patients undergoing injection of cultured corneal endothelial cells for corneal endothelial failure. *Ophthalmology*. 2021;128(4):504–514.